Published in final edited form as:

*Phys Med Biol*. ; 66(5): . doi:10.1088/1361-6560/abe050.

# Comparison of weekly and daily online adaptation for head and neck intensity-modulated proton therapy

**Mislav Bobić**[1,2], **Arthur Lalonde**[1,3], **Gregory C. Sharp**[1,3], **Clemens Grassberger**[1,3], **Joost M. Verburg**[1,3], **Brian A. Winey**[1,3], **Antony J. Lomax**[2,4], **Harald Paganetti**[1,3]

[1]Department of Radiation Oncology, Massachusetts General Hospital, Boston, Massachusetts, USA,

[2]ETH Zürich, Zürich, Switzerland,

[3]Harvard Medical School, Boston, Massachusetts, USA,

[4]Paul Scherrer Institute, Villigen, Switzerland

## Abstract

The high conformality of intensity-modulated proton therapy (IMPT) dose distributions causes treatment plans to be sensitive to geometrical changes during the course of a fractionated treatment. This can be addressed using adaptive proton therapy (APT). One important question in APT is the frequency of adaptations performed during a fractionated treatment, which is related to the question whether plan adaptation has to be done online or offline. The purpose of this work is to investigate the impact of weekly and daily online IMPT plan adaptation on the treatment quality for head and neck patients. A cohort of ten head and neck patients with daily acquired cone-beam CT (CBCT) images was evaluated retrospectively. Dose tracking of the IMPT treatment was performed for three scenarios: base plan with no adaptation (BP), weekly online adaptation ($OA_W$), and daily online adaptation ($OA_D$). Both adaptation schemes used an in-house developed online APT workflow, performing Monte Carlo (MC) dose calculations on scatter-corrected CBCTs. IMPT plan adaptation was achieved by only tuning the weights of a subset of beamlets, based on deformable image registration from the planning CT to each CBCT. Although $OA_D$ mitigated random delivery errors more effectively than $OA_W$ on a fraction per fraction basis, both $OA_W$ and $OA_D$ achieved the clinical goals for all ten patients, while BP failed for six cases. In the high-risk CTV, accumulated values of $D_{98\%}$ ranged between 97.15% and 99.73% of the prescription dose for $OA_D$, with a median of 98.07%. For $OA_W$, values between 95.02% and 99.26% were obtained, with a median of 97.61% of the prescription dose. Otherwise, the dose to most organs at risk was similar for all three scenarios. Globally, our results suggest that $OA_W$ could be used as an alternative approach to $OA_D$ for most patients in order to reduce the clinical workload.

### Keywords

proton therapy; adaptive radiotherapy; head and neck cancer; cone-beam CT; Monte Carlo

## 1. Introduction

Head and neck (H&N) cancer patients often present challenging cases for treatment with radiation therapy due to the proximity of target volumes to organs at risk (OARs), such as the spinal cord, larynx, parotid glands, or others. These cases benefit from steep dose gradients in the planned dose distribution, which allow for highly localized doses in the clinical target volume (CTV) while avoiding the surrounding OARs. Intensity-modulated proton therapy (IMPT) can create such steep dose gradients and, therefore, has the potential of reducing the dose deposited to healthy tissue compared to photon radiotherapy, while providing equivalent target coverage (Miralbell *et al* 2000, Barten *et al* 2015, Blanchard *et al* 2016, Leeman *et al* 2017, Moreno *et al* 2019). However, sharp dose gradients created by IMPT are highly sensitive to geometrical changes in the patient, which may degrade the overall treatment quality (Lomax 2008b, Paganetti 2012, Góra *et al* 2015, Müller *et al* 2015, Szeto *et al* 2016, Stützer *et al* 2017). Since radiation therapy treatment plans are designed based on an initial simulation CT scan for planning, various error sources might occur during a fractionated treatment and distort the dose distribution actually delivered to the patient. These errors include patient set-up variations and day-to-day (i.e., interfractional) anatomy changes.

Set-up variations are caused by inconsistent positioning of the patient on the treatment couch compared to the patient's original position and posture recorded on the planning CT. Such set-up variations usually lead to random errors in dose delivery between fractions. Interfractional anatomy changes can have several sources, out of which weight loss and tumor shrinkage are especially relevant for patients receiving H&N cancer treatment (Beaver *et al* 2001, Wu *et al* 2009, Elstrøm *et al* 2010). In contrast to random set-up variations, which typically lead to blurring of the delivered dose distribution, weight loss and tumor shrinkage often result in systematic errors and can severely impact the treatment quality. This is especially true for IMPT plans due to the finite range of individual proton beamlets.

To account for uncertainties and potential delivery errors throughout the treatment, additional margins are applied around the target volume during treatment planning to ensure proper tumor coverage for all fractions. While target margins increase the probability of the tumor receiving its prescribed dose, they also inevitably raise the overall integral dose to healthy tissue and OARs, increasing the risk for side effects. Moreover, simply expanding the prescription dose-volume does not guarantee sufficient target coverage for all fractions due to unforeseeable changes in patient anatomy throughout the treatment. As an alternative, robust IMPT optimization can be performed when creating a treatment plan by explicitly considering different uncertainty sources during the optimization process (Liu *et al* 2013, van Dijk *et al* 2016, Unkelbach *et al* 2018). The resulting robust plan is substantially less sensitive to the considered uncertainties and will deliver a clinically acceptable dose distribution, as long as the deviations from the original planning scenario do not exceed a certain level. As reported in the cited studies, robust optimization typically outperforms plans that utilize the simple target margin approach in terms of treatment quality. However, the increased plan robustness is usually realized by smoothing dose gradients in the target region. As a consequence, the integral dose to healthy tissue and OARs is yet again

increased (Chen *et al* 2012, van de Water *et al* 2016), diminishing some of the potential dosimetric benefits provided by IMPT.

Since both target margins and robust optimization account for delivery uncertainties at the cost of an increased dose deposited in the surrounding healthy tissue, adaptive proton therapy (APT) presents a viable solution to maintain the benefits of IMPT, consistent target dose and reduced OAR dose, throughout a fractionated treatment (Simone *et al* 2011, Kurz *et al* 2016b, Veiga *et al* 2016, Bernatowicz *et al* 2018, Botas *et al* 2018, van de Water *et al* 2018, Nenoff *et al* 2019, Albertini *et al* 2020). APT can either be performed offline, which often involves a complete treatment re-planning on a new set of contours should the original plan not meet the clinical objectives, or online, i.e., while the patient is positioned on the treatment couch and ready for beam delivery. Since online APT can respond more rapidly to the changes in patient anatomy, it has the advantage of not interrupting and delaying the treatment, as well as the capability to account for set-up variations of the patient at each fraction. The latter could allow for target margin reduction, potentially reducing the integral dose to healthy tissue.

A study published previously by our group reports a significant improvement in treatment quality for H&N cases utilizing an online APT approach (Botas *et al* 2018). The online adaptation workflow in that work was performed based on Monte Carlo (MC) dose calculation and cone-beam CT (CBCT) images, which are routinely acquired in some proton therapy centers for daily patient alignment and positioning (Hua *et al* 2017, Landry and Hua 2018). However, this study assumed a daily adaptation scheme and did not address the impact of adaptation frequency on the treatment quality. While the clinical implementation of daily adaptation could be feasible based on the reported time requirements (~5 minutes per fraction), a less frequent adaptation scheme might be sufficient for systematic delivery errors caused by, e.g., weight loss and tumor shrinkage. The overall increase in treatment time induced by online APT could represent a burden for some patients lying still on the couch and waiting to complete the fraction, therefore decreasing the number of adapted fractions would favorably reduce the clinical workload.

In this study, we investigate the impact of adaptation frequency on the treatment quality for H&N patients receiving IMPT by directly comparing weekly online adaptation ($OA_W$) with daily online adaptation ($OA_D$). The main goal is to analyze how decisive the added value is in terms of plan quality if one invests the time and resources for $OA_D$. Both adaptation schemes are also compared with the unadapted base plan (BP) scenario. A representative cohort of ten H&N patients with daily acquired CBCTs was considered by evaluating the target coverage and OAR sparing throughout the treatment.

## 2. Methods and Materials

### 2.1 Patient cohort

A representative cohort of ten H&N patients with daily acquired CBCTs was considered in this retrospective study. The tumor locations include the oral cavity, oropharynx, and larynx. Since at the time of this study, CBCT imaging was not available for our proton patients, the analysis was based on patients originally treated with volumetric modulated arc

therapy (VMAT). The number of CBCTs per patient ranged between 31 and 35 image sets (i.e., fractions), for a total of 320 analyzed scenarios. The CBCTs were acquired with an Elekta XVI system using a 100 kVp tube voltage, 10 ms exposure, and 10 mA tube current. The acquisition was performed with a centered panel position over 220 degrees, a 20 cm collimator, and no bowtie filter.

For each patient, a planning CT was available with the corresponding planning contours, delineated by an experienced oncologist. Both a high-risk CTV and a low-risk CTV were defined in each structure set. The high-risk CTVs included the primary tumor and the adjacent high-risk lymph nodes, while the low-risk CTVs covered bilateral lymph nodes considered at risk for subclinical disease. Furthermore, contours of the spinal cord, parotid glands, constrictor muscles, larynx, brainstem, esophagus, and oral cavity were classified as OARs.

## 2.2 Treatment planning

An IMPT plan was created for each patient using RayStation (v8.99, RaySearch Laboratories, Stockholm, Sweden). The treatment plans were designed and optimized with a simultaneous integrated boost (SIB) technique, where the prescribed mean dose was set to 57 Gy(RBE) and 70 Gy(RBE) for the low-risk CTV and high-risk CTV, respectively. For both CTVs, the following objectives were defined: $D_{98} \geq 95\%$ and $D_2 \leq 107\%$ of the prescribed dose, where $D_{98}$ and $D_2$ are the minimum doses to 98% and 2% of the target volume, respectively. For the OARs, the following constraints regarding the mean dose ($D_{mean}$) or maximum dose ($D_{max}$) were applied: $D_{max} < 45$ Gy for the spinal cord, $D_{mean} < 26$ Gy for both parotid glands, $D_{mean} < 42$ Gy for the constrictor muscles, $D_{mean} < 40$ Gy for the larynx, and $D_{max} < 54$ Gy for the brainstem. All plans were optimized to deliver the prescribed dose to the CTVs using multi-criteria optimization (MCO), with objectives set to separately minimize the generalized equivalent uniform dose (gEUD) to the defined OARs, in addition to the esophagus and oral cavity. The goal of this study was to demonstrate the effectiveness of adaptive strategies to ensure coverage of a defined target volume. In order to do so independent of institution or planner dependent margins, we decided to use the CTV. Furthermore, no robust optimization was employed during treatment planning, resulting in sharper dose gradients around the target volume and deliberately creating a more challenging case for the adaptation algorithm.

All ten IMPT plans were created with our clinical proton beam template: three fields originating from different gantry angles (60°, 180°, and 300°), each using a range shifter with a corresponding water equivalent thickness (WET) of 40 mm and a 30 mm minimum air gap. The proton beam specifications were based on the *IBA Dedicated Nozzle* beam model, with the spot sigma ($\sigma$) in air ranging from 2.5 mm to 6.4 mm for the applicable nominal beam energies (between 225 MeV and 65 MeV, respectively). Dose calculations and optimization during treatment planning were performed using the Monte Carlo algorithm in RayStation on a $2.0 \times 2.0 \times 2.0$ $mm^3$ dose grid, assuming a constant relative biological effectiveness (RBE) equal to 1.1.

### 2.3 Image pre-processing

An essential requirement for online APT is the acquisition of volumetric images of the positioned patient, providing information on the patient's set-up and anatomy of the day. This information can be obtained by acquiring a CBCT scan immediately before beam delivery. The online APT algorithm then requires a deformation vector field (VF) calculated between the planning CT and the CBCT to adjust the treatment plan parameters based on the discrepancies between the two image sets. Before calculating the deformation VFs, the image quality of the CBCTs was improved using a scatter-correction technique.

In APT, the dose calculation can either be done on a virtual CT (vCT) by deforming the planning CT to the daily CBCT (Landry *et al* 2015, Veiga *et al* 2015, Kurz *et al* 2016a, Thummerer *et al* 2020) or on the CBCT directly if the necessary corrections to the image quality are applied (Kurz *et al* 2015, 2019, Park *et al* 2015, Lalonde *et al* 2020). For this work, the latter approach was realized. The main contributor to the unsatisfactory image quality of CBCTs is X-ray scatter originating from the patient and the detector panel. As a result, the reconstructed image sets provide a compromised Hounsfield unit (HU) accuracy. To reduce the resulting image artifacts and restore HU accuracy, our CBCTs were scatter-corrected in the projection domain using a U-shape deep convolutional neural network (DCNN) trained to reproduce Monte Carlo calculated scatter distributions (Lalonde *et al* 2020). This technique was validated using a method developed specifically for proton dose calculations on CBCT images for APT (Park *et al* 2015).

Following scatter correction, the daily CBCTs were aligned to the plan isocenter by performing rigid registration from the CBCT to the planning CT. This step was achieved using Plastimatch, an open-source tool for medical imaging and radiotherapy image processing (Sharp *et al* 2010, Shackleford *et al* 2012). The rigid registration was done based on the target volumes within the patient instead of registering based on the entire image. This was realized by defining an extended bounding box around the target volume contour (high-risk CTV plus low-risk CTV) and then calculating the six degrees of freedom (6-DOF) VF only for the image information inside the bounding box. The calculated 6-DOF VF is then applied to the whole CBCT image, matching it to the planning CT. The extension of the bounding box around the target volume was set to 20 mm in each dimension. This alignment of the CBCT to the planning CT imitates the clinical routine, where the medical staff uses the CBCT scan to verify the patient's position during treatment by applying a 6-DOF shift of the treatment couch.

The scatter-corrected and aligned CBCT images were used for deformable image registration (DIR) of the planning CT for each fraction. DIR was performed with the GPU parallelized B-spline algorithm in Plastimatch. The calculated deformation VFs map the original planning CT to each CBCT and, as such, were used to propagate the planning contours to each CBCT. The accuracy of the propagated structures had to be visually verified on the CBCT image, as there is no automated and robust method to validate the structure contours for H&N scans (Li *et al* 2017, Botas *et al* 2018). Furthermore, the deformation VFs were later inverted to track the dose accumulated throughout the treatment by deforming the dose distribution of each fraction back to the planning CT.

Two final modifications of the CBCTs were performed before launching dose calculations for the online APT workflow. First, image artifact regions caused by the patient's dental filling of each CBCT were masked with the propagated artifact contour, setting a constant HU value of 26 – this was done to imitate the procedure implemented in RayStation. Second, the CBCT image was supplemented with the CT image to fill in the potentially missing information of the external patient anatomy, caused by the limited field of view (FOV) of the CBCT scans. To clarify, there were cases where some of the planned proton beamlets missed part of the patient's skin, as it was not acquired by the reduced FOV of the CBCT. As a mitigation method, the volume beyond the CBCT FOV was complemented with the planning CT. The resulting images were verified visually and used for dose calculations during the online APT workflow.

### 2.4 Online plan adaptation

IMPT plan adaptation was performed with an in-house developed online APT framework employing GPU-accelerated Monte Carlo (gPMC) for dose calculations (Jia *et al* 2011, 2012, Giantsoudi *et al* 2015, Qin *et al* 2016). Compared to analytical dose calculations, MC significantly improves the accuracy in proton therapy, which is especially true for treatment sites that exhibit considerable tissue heterogeneities (Lomax 2008a, Paganetti 2012, Grassberger *et al* 2014, Schuemann *et al* 2015), such as H&N cases. As described earlier, each daily scatter-corrected CBCT received a new set of contours for dose scoring based on which plan adaptation was performed. For each CBCT, a dose-influence matrix was calculated with gPMC to derive the dose contributed by each proton beamlet of the treatment plan. To increase computational efficiency, the dose-influence matrices were only scored in regions of interest defined by the propagated contours (target volumes and OARs).

Plan adaptation based on a complete re-planning might result in the best plan possible at any given fraction. However, it may require quality assurance as beamlet distributions (weights and energies), as well as range shifter requirements might change. As we aim at a first adaptive workflow while the patient is prepared for treatment, we decided to allow only changes in weight for a subset of beamlets without changing their positions or energies. This approach reduced the complexity of the required adaptations because it does not modify the plan's number of energy layers, increasing the deliverability of the adapted plans. This method might be considered a delivery correction instead of plan re-optimization – a distinction with potential impact on clinical workflow guidelines.

Based on the calculated dose-influence matrices, an in-house developed radiotherapy optimization algorithm (Trofimov *et al* 2005) was employed for beamlet weight re-optimization. The optimization was performed according to the same objectives as for the nominal treatment plans. Beamlet weight tuning was applied to the smallest set of beamlets carrying at least 33% of the total beam's weight, whereby the number of selected beamlets had to comprise at least 10% of the total number of beamlets. Finally, the adapted plans were verified by performing dose calculations on CBCTs with gPMC and scoring the dose for the propagated contours.

### 2.5 Evaluation metrics

Two adaptation frequencies were evaluated and compared: daily online adaptation ($OA_D$) and weekly online adaptation ($OA_W$). $OA_D$ was applied by performing online adaptation of the nominal treatment plan at each fraction to achieve the defined clinical objectives for that fraction. $OA_W$ was realized by performing the same adaptation approach on the first available day of each week, and then using the adapted plan for all fractions during the rest of the week (i.e., until the next weekly adaptation). Both adaptation schemes were also compared with the unadapted base plan (BP) scenario. Out of the 320 fractions, 79 were adapted for the $OA_W$ scheme (24.7% of the total). On average, almost every $4^{th}$ fraction was adapted instead of every $5^{th}$ during a weekly schedule because most patients did not receive treatment on each day of the week.

The evaluation of all IMPT plans was based on the calculated dose-volume histograms (DVH) and their corresponding metrics. In particular, the $D_{98}$ and $D_2$ of the high-risk CTVs, as well as the $D_{98}$ of the low-risk CTVs, were analyzed to evaluate the target coverage (all in % of the prescription dose). This evaluation was done both for individual fractions and for the dose accumulated throughout the treatment. Dose accumulation was achieved by inverting and applying each deformation VF to its corresponding fraction dose distribution and then scoring the deformed dose in the planning contours, effectively tracking the cumulative dose. Furthermore, the dose accumulated in OARs was analyzed by evaluating their relevant dosimetric values ($D_{mean}$ or $D_{1cc}$, both in Gy(RBE)). The $D_{1cc}$ is used as an alternative metric to $D_{max}$ for evaluation of the spinal cord and brainstem to decrease the sensitivity to noise.

## 3. Results and Discussion

The performance of the three delivery scenarios is first analyzed for the dose per fraction. In figure 1, the evolution of the target coverage delivered for individual fractions throughout the treatment is presented for three representative patients. The displayed cases were selected due to their suitability to represent different observations made for all patients. The BP scenario for patient A exhibits a systematic degradation of the target coverage over the course of treatment. The weight loss was also noticeable in the CBCTs. Patient B, on the other hand, shows random fluctuations caused by anatomical positioning inconsistencies with the planning CT. The $D_{98}$ for the high-risk CTV indicates a worse performance of $OA_W$ than BP for individual fractions, especially for the fifth week of treatment. Finally, patient C exhibits no clear trend throughout the treatment with very low fluctuations. Overall, $OA_D$ achieves the best target coverage, whereby both $OA_D$ and $OA_W$ outperform BP.

The main take away from figure 1 is the occurrence of systematic and random delivery errors over the course of a fractionated treatment and their impact on online adaptation schemes. We observe that both $OA_W$ and $OA_D$ are capable of mitigating systematic errors caused by patient weight loss or tumor shrinkage, while random errors caused by daily positioning and anatomy variations are only effectively accounted for by $OA_D$. In some cases, $OA_W$ even led to a worse week of treatment than BP in terms of target coverage (e.g., $5^{th}$ week for patient B). This can occur if the weekly adaptation is performed on a

fraction during which the patient's position substantially deviates from the regular treatment position.

While the results depicted in figure 1 suggest the superiority of $OA_D$ over $OA_W$, the dose accumulated throughout the treatment may serve as a clinically more meaningful evaluation. Figure 2 shows DVHs of the same three patients, comparing the cumulative doses of all three delivery scenarios. $OA_D$ and $OA_W$ achieve very similar target coverages for patients A and C, while a noticeable difference can be observed for the high-risk CTV of patient B. For this patient, $OA_W$ barely reached the clinical objective defined for the high-risk CTV ($D_{98}$ = 95.0%, which exactly matches the objective). The dose to the low-risk CTVs delivered by $OA_W$ and $OA_D$ achieved the clinical objectives for all three patients.

Although $OA_W$ did not achieve all defined clinical objectives for every individual fraction (see figure 1), all three patients received a clinically acceptable cumulative dose at the end of treatment. The reason for this outcome is the impact of the previously discussed systematic and random delivery errors on the treatment plan quality. While random errors typically result in blurring of the delivered dose distribution, systematic errors can result in severe underdosing of the tumor. Systematic errors are, therefore, by far more decisive when considering uncertainties, especially for proton therapy due to the finite range of proton beamlets. The capability of $OA_W$ to mitigate systematic delivery errors is the reason why the resulting accumulated dose distributions show similar performances for both adaptation schemes.

Figure 3 presents a more insightful comparison of the cumulative dose distributions delivered by $OA_W$ and $OA_D$ for the three representative patients. The axial CT slices displayed in the figure were selected by locating relevant regions with the highest discrepancies between the two adaptation schemes. Figure 3 a) shows the cumulative isodose lines of $OA_W$ and $OA_D$, both represented by 95% of the prescribed dose for the high-risk CTV and low-risk CTV, yielding 66.5 Gy and 54.1 Gy, respectively. Overall, the corresponding isodoses match each other very closely, apart from patient B, where $OA_W$ fails to cover a part of the high-risk CTV in the neck region (compare with DVH in figure 2). The difference between $OA_W$ and $OA_D$ in that region is also evident in figure 3 b), which depicts subtracted dose maps of the two adaptation schemes ($OA_D$ minus $OA_W$) for the same CT slices as in figure 3 a). Patients A and B exhibit differences of up to 4 Gy outside and inside the target volume, respectively, while patient C shows minimal differences between $OA_D$ and $OA_W$.

The overall results regarding target coverage for all ten patients were summarized in boxplots, as seen in figure 4. The evaluated dosimetric data are presented for the three delivery scenarios, both for the dose delivered per individual fractions (320 data points) and for the cumulative dose (10 data points). The dashed lines indicate the clinical objectives set for the target coverage. Supporting the previously observed results from figure 1, $OA_W$ exhibits substantial fluctuations compared to $OA_D$ when scored on individual fractions, presumably due to daily positioning and anatomy variations (i.e., random errors). For the dose accumulated at the end of treatment, however, $OA_D$ and $OA_W$ yield comparable target coverages. Both adaptation schemes achieved the defined clinical objectives for all ten

patients, whereby, for $OA_W$, one case barely passed the required 95% for the $D_{98}$ of the high-risk CTV (see figures 2 and 3, patient B). This case is indicated as an outlier in the boxplot. The boxplots representing the $D_{98}$ of the low-risk CTVs are well above the clinical objective for both adaptation schemes. The unadapted BP scenario yields substantially worse results in all aspects due to underdosing of both the high-risk and low-risk CTVs for multiple patients.

As for the OARs, both adaptation schemes show comparable performances (see figure 2). Compared to BP, both $OA_D$ and $OA_W$ improved the delivered plan qualities in all aspects, increasing target coverage and OAR sparing. Similar to the cumulative target dose in figure 4, the dose accumulated throughout treatment in OARs and their relevant dosimetric values are presented in figure 5. $OA_D$ and $OA_W$ show similar results for all OARs, including the integral dose to the healthy tissue. The displayed boxplots include all evaluated structures, even if they were excluded from optimization due to their proximity to the target volume, reflected by the outliers far above the clinical constraints (see parotid glands and constrictor muscles). Compared to both adaptation scenarios, BP yields worse OAR sparing for all evaluated structures. The brainstem is not included in the figure because its received dose was low in all cases. This is seen in table 1, which summarizes dose distribution statistics evaluated for all structures (targets and OARs). Based on the results presented in figure 5 and table 1, there is no clear advantage of $OA_D$ over $OA_W$ in terms of OAR sparing and integral dose.

In summary, our results demonstrate comparable performances by the two adaptation schemes, both in terms of target coverage and OAR sparing. The median $D_{98}$ for the high-risk CTV was 97.61% and 98.07% of the prescription dose for $OA_W$ and $OA_D$, respectively, while for the low-risk CTV, we obtained 97.60% and 97.97% for the same metrics. One outlier was observed for $OA_W$ due to a substantially lower coverage of the high-risk CTV compared to $OA_D$, resulting from daily positioning variations between fractions (patient B). Nevertheless, both $OA_D$ and $OA_W$ were able to meet the clinical goals for the two CTVs of all ten patients, while the unadapted BP scenario failed for six out of ten cases. In terms of OAR sparing, both adaptation schemes showed notably similar results for all structures, as well as a reduced dose compared to BP, as seen in table 1. The integral dose to healthy tissue remained comparable for all delivery scenarios. It should be noted that the BP optimization was performed on the CTV without additional target margins because our primary goal was to compare weekly with daily adaptation. For our purpose, the BP scenario serves to demonstrate the plan degradation in a fractionated treatment if no adaptation is applied. Furthermore, it shows that there is a clear difference between no adaptation and the occasional weekly adaptation.

The fact that robust optimization was not employed during treatment planning also has an impact on our results. Similar to the previously discussed absence of target margins, the BP scenario without robust optimization is disadvantaged compared to the two adaptation schemes. Furthermore, this will also slightly disadvantage the $OA_W$ scenario compared to $OA_D$. For $OA_W$, the absence of robust optimization increases its sensitivity to daily positioning and random anatomy variations, which is reflected by the fluctuations observed in figure 1. This does not present an issue for $OA_D$, where robust optimization would

increase the integral dose due to less sharp dose gradients. To base the comparison between $OA_D$ and $OA_W$ only on adaptation frequency, we decided to exclude robust optimization from both adaptation schemes and, therefore, created only one plan as an initial starting point for each patient.

Since dose calculation was performed on scatter-corrected CBCTs, the results for the BP might slightly suffer from range errors as the initial plans were optimized on the CT. The extent of these range errors comes down to the HU accuracy of the corrected CBCTs. The method we applied for scatter-correction was reported to yield a 3%/3mm gamma passing rate of 98.72% for experimental CBCT patient images (Lalonde *et al* 2020). It should be noted that, in figure 1, these residual range errors may result in an offset of the evaluated metrics for BP, which does not justify the observed degradation trends and high fluctuations.

The observed results suggest that a reduced number of adaptations might be sufficient instead of $OA_D$ to reduce the clinical workload and increase patient comfort throughout the treatment. Although $OA_D$ delivered superior dose distributions in terms of target coverage, $OA_W$ achieved the same clinical goals while reducing the number of adaptations and the time required in the clinical workflow. For our patient cohort, $OA_D$ required between 8 and 22 minutes to adapt the plans for each individual fraction, with a median adaptation time of 12 minutes, out of which MC dose calculation and optimization were the most demanding steps. This could be reduced with optimized hardware and software architecture. The reason for the increased adaptation time compared to our previous study (Botas *et al* 2018) is the higher number of beamlets planned to cover both target volumes. Another challenge that will need to be addressed is quality assurance (QA) of the adapted plans. In addition to reduced time requirements, adapting weekly instead of daily would allow for an easier QA.

## 4. Conclusion

We evaluated the impact of online adaptation frequency on the plan quality for H&N patients receiving IMPT treatment by comparing weekly online adaptation ($OA_W$) with daily online adaptation ($OA_D$). Most importantly, we performed adaptation by only adjusting the weights of a subset of beamlets instead of reoptimizing plans, thus accomplishing transparent plan adjustments. Our results revealed a notably similar performance of $OA_W$ compared to $OA_D$. The median $D_{98}$ for the high-risk CTV was 97.61% and 98.07% of the prescribed dose for $OA_W$ and $OA_D$, respectively, while the low-risk CTV reached 97.60% and 97.97% for the same metrics. In terms of OAR sparing, both adaptation schemes showed a comparable performance for all structures. In conclusion, our study suggests that $OA_W$ could be employed as an alternative approach to $OA_D$ to reduce the clinical workload and increase patient comfort throughout treatment.

## Acknowledgements

The authors would like to thank RaySearch Laboratories (Stockholm, Sweden) for providing a non-clinical software license for the RayStation treatment planning system. This work was funded by the National Cancer Institute (NCI R01 229178).

## REFERENCES


Albertini F, Matter M, Nenoff L, Zhang Y and Lomax A 2020 Online daily adaptive proton therapy The British Journal of Radiology 93 20190594 [PubMed: 31647313]

Barten DLJ, Tol JP, Dahele M, Slotman BJ and Verbakel WFAR 2015 Comparison of organ-at-risk sparing and plan robustness for spot-scanning proton therapy and volumetric modulated arc photon therapy in head-and-neck cancer Medical Physics 42 6589–98 [PubMed: 26520750]

Beaver ME, Matheny KE, Roberts DB and Myers JN 2001 Predictors of Weight Loss During Radiation Therapy Otolaryngology–Head and Neck Surgery 125 645–8 [PubMed: 11743469]

Bernatowicz K, Geets X, Barragan A, Janssens G, Souris K and Sterpin E 2018 Feasibility of online IMPT adaptation using fast, automatic and robust dose restoration Physics in Medicine & Biology 63 085018 [PubMed: 29595145]

Blanchard P et al. 2016 Intensity-modulated proton beam therapy (IMPT) versus intensity-modulated photon therapy (IMRT) for patients with oropharynx cancer – A case matched analysis Radiotherapy and Oncology 120 48–55 [PubMed: 27342249]

Botas P, Kim J, Winey B and Paganetti H 2018 Online adaption approaches for intensity modulated proton therapy for head and neck patients based on cone beam CTs and Monte Carlo simulations Physics in Medicine & Biology 64 015004 [PubMed: 30524097]

Chen W, Unkelbach J, Trofimov A, Madden T, Kooy H, Bortfeld T and Craft D 2012 Including robustness in multi-criteria optimization for intensity-modulated proton therapy Physics in Medicine and Biology 57 591–608 [PubMed: 22222720]

van Dijk LV, Steenbakkers RJHM, ten Haken B, van der Laan HP, van ‘t Veld AA, Langendijk JA and Korevaar EW 2016 Robust Intensity Modulated Proton Therapy (IMPT) Increases Estimated Clinical Benefit in Head and Neck Cancer Patients ed S-Y Sung PLOS ONE 11 e0152477 [PubMed: 27030987]

Elstrøm UV, Wysocka BA, Muren LP, Petersen JBB and Grau C 2010 Daily kV cone-beam CT and deformable image registration as a method for studying dosimetric consequences of anatomic changes in adaptive IMRT of head and neck cancer Acta Oncologica 49 1101–8 [PubMed: 20831502]

Giantsoudi D, Schuemann J, Jia X, Dowdell S, Jiang S and Paganetti H 2015 Validation of a GPU-based Monte Carlo code (gPMC) for proton radiation therapy: clinical cases study Physics in Medicine and Biology 60 2257–69 [PubMed: 25715661]

Góra J, Kuess P, Stock M, Andrzejewski P, Knäusl B, Paskeviciute B, Altorjai G and Georg D 2015 ART for head and neck patients: On the difference between VMAT and IMPT Acta Oncologica 54 1166–74 [PubMed: 25850583]

Grassberger C, Daartz J, Dowdell S, Ruggieri T, Sharp G and Paganetti H 2014 Quantification of Proton Dose Calculation Accuracy in the Lung International Journal of Radiation Oncology*Biology*Physics 89 424–30

Hua C, Yao W, Kidani T, Tomida K, Ozawa S, Nishimura T, Fujisawa T, Shinagawa R and Merchant TE 2017 A robotic C-arm cone beam CT system for image-guided proton therapy: design and performance The British Journal of Radiology 90 20170266 [PubMed: 28830239]

Jia X, Gu X, Graves YJ, Folkerts M and Jiang SB 2011 GPU-based fast Monte Carlo simulation for radiotherapy dose calculation Physics in Medicine and Biology 56 7017–31 [PubMed: 22016026]

Jia X, Schümann J, Paganetti H and Jiang SB 2012 GPU-based fast Monte Carlo dose calculation for proton therapy Physics in Medicine and Biology 57 7783–97 [PubMed: 23128424]

Kurz C, Dedes G, Resch A, Reiner M, Ganswindt U, Nijhuis R, Thieke C, Belka C, Parodi K and Landry G 2015 Comparing cone-beam CT intensity correction methods for dose recalculation in adaptive intensity-modulated photon and proton therapy for head and neck cancer Acta Oncologica 54 1651–7 [PubMed: 26198654]

Kurz C et al. 2016a Investigating deformable image registration and scatter correction for CBCT-based dose calculation in adaptive IMPT Medical Physics 43 5635–46 [PubMed: 27782706]

Kurz C, Nijhuis R, Reiner M, Ganswindt U, Thieke C, Belka C, Parodi K and Landry G 2016b Feasibility of automated proton therapy plan adaptation for head and neck tumors using cone beam CT images Radiation Oncology 11

Kurz C, Maspero M, Savenije MHF, Landry G, Kamp F, Pinto M, Li M, Parodi K, Belka C and van den Berg CAT 2019 CBCT correction using a cycle-consistent generative adversarial network and unpaired training to enable photon and proton dose calculation Physics in Medicine & Biology 64 225004 [PubMed: 31610527]

Lalonde A, Winey BA, Verburg JM, Paganetti H and Sharp GC 2020 Evaluation of CBCT scatter correction using deep convolutional neural networks for head and neck adaptive proton therapy Physics in Medicine & Biology accepted 10.1088/1361-6560/ab9fcb

Landry G and Hua C 2018 Current state and future applications of radiological image guidance for particle therapy Medical Physics 45

Landry G et al. 2015 Investigating CT to CBCT image registration for head and neck proton therapy as a tool for daily dose recalculation Medical Physics 42 1354–66 [PubMed: 25735290]

Leeman JE, Romesser PB, Zhou Y, McBride S, Riaz N, Sherman E, Cohen MA, Cahlon O and Lee N 2017 Proton therapy for head and neck cancer: expanding the therapeutic window The Lancet Oncology 18 e254–65 [PubMed: 28456587]

Li X, Zhang Y, Shi Y, Wu S, Xiao Y, Gu X, Zhen X and Zhou L 2017 Comprehensive evaluation of ten deformable image registration algorithms for contour propagation between CT and cone-beam CT images in adaptive head & neck radiotherapy PloS one 12 e0175906 [PubMed: 28414799]

Liu W, Mohan R, Zhang X, Zhu XR and Frank SJ 2013 Effectiveness of Robust Optimization in Oropharynx IMPT Planning International Journal of Radiation Oncology*Biology*Physics 87 S443

Lomax AJ 2008a Intensity modulated proton therapy and its sensitivity to treatment uncertainties 1: the potential effects of calculational uncertainties Physics in Medicine and Biology 53 1027–42 [PubMed: 18263956]

Lomax AJ 2008b Intensity modulated proton therapy and its sensitivity to treatment uncertainties 2: the potential effects of inter-fraction and inter-field motions Physics in Medicine and Biology 53 1043–56 [PubMed: 18263957]

Miralbell R, Cella L, Weber D and Lomax A 2000 Optimizing radiotherapy of orbital and paraorbital tumors: intensity-modulated X-ray beams vs. intensity-modulated proton beams International Journal of Radiation Oncology*Biology*Physics 47 1111–9

Moreno AC et al. 2019 Intensity modulated proton therapy (IMPT) – The future of IMRT for head and neck cancer Oral Oncology 88 66–74 [PubMed: 30616799]

Müller BS, Duma MN, Kampfer S, Nill S, Oelfke U, Geinitz H and Wilkens JJ 2015 Impact of interfractional changes in head and neck cancer patients on the delivered dose in intensity modulated radiotherapy with protons and photons Physica Medica 31 266–72 [PubMed: 25724350]

Nenoff L, Matter M, Hedlund Lindmar J, Weber DC, Lomax AJ and Albertini F 2019 Daily adaptive proton therapy – the key to innovative planning approaches for paranasal cancer treatments Acta Oncologica 58 1423–8 [PubMed: 31364904]

Paganetti H 2012 Range uncertainties in proton therapy and the role of Monte Carlo simulations Physics in Medicine and Biology 57 R99–R117 [PubMed: 22571913]

Park Y-K, Sharp GC, Phillips J and Winey BA 2015 Proton dose calculation on scatter-corrected CBCT image: Feasibility study for adaptive proton therapy Medical Physics 42 4449–59 [PubMed: 26233175]

Qin N, Botas P, Giantsoudi D, Schuemann J, Tian Z, Jiang SB, Paganetti H and Jia X 2016 Recent developments and comprehensive evaluations of a GPU-based Monte Carlo package for proton therapy Physics in Medicine and Biology 61 7347–62 [PubMed: 27694712]

Schuemann J, Giantsoudi D, Grassberger C, Moteabbed M, Min CH and Paganetti H 2015 Assessing the Clinical Impact of Approximations in Analytical Dose Calculations for Proton Therapy International Journal of Radiation Oncology*Biology*Physics 92 1157–64

Shackleford JA, Shusharina N, Verberg J, Warmerdam G, Winey B, Neuner M, Steininger P, Arbisser A, Golland P and Lou Y 2012 Plastimatch 1.6 – current capabilities and future directions MICCAI, First International Workshop on Image-Guidance and Multimodal Dose Planning in Radiation Therapy

Sharp GC, Li R, Wolfgang J, Chen G, Peroni M, Spadea MF, Mori S, Zhang J, Shackleford J and Kandasamy N 2010 Plastimatch – an open source software suite for radiotherapy image processing Proceedings of the XVI'th International Conference on the use of Computers in Radiotherapy (ICCR), Amsterdam, Netherlands

Simone CB, Ly D, Dan TD, Ondos J, Ning H, Belard A, O'Connell J, Miller RW and Simone NL 2011 Comparison of intensity-modulated radiotherapy, adaptive radiotherapy, proton radiotherapy, and adaptive proton radiotherapy for treatment of locally advanced head and neck cancer Radiotherapy and Oncology 101 376–82 [PubMed: 21663988]

Stützer K, Jakobi A, Bandurska-Luque A, Barczyk S, Arnsmeyer C, Löck S and Richter C 2017 Potential proton and photon dose degradation in advanced head and neck cancer patients by intratherapy changes Journal of Applied Clinical Medical Physics 18 104–13

Szeto YZ, Witte MG, van Kranen SR, Sonke J-J, Belderbos J and van Herk M 2016 Effects of anatomical changes on pencil beam scanning proton plans in locally advanced NSCLC patients Radiotherapy and Oncology 120 286–92 [PubMed: 27393217]

Thummerer A et al. 2020 Comparison of the suitability of CBCT- and MR-based synthetic CTs for daily adaptive proton therapy in head and neck patients Physics in Medicine & Biology accepted 10.1088/1361-6560/abb1d6

Trofimov A, Rietzel E, Lu H-M, Martin B, Jiang S, Chen GTY and Bortfeld T 2005 Temporo-spatial IMRT optimization: concepts, implementation and initial results Physics in Medicine and Biology 50 2779–98 [PubMed: 15930602]

Unkelbach J et al. 2018 Robust radiotherapy planning Physics in Medicine & Biology 63 22TR02

Veiga C, Alshaikhi J, Amos R, Lourenço AM, Modat M, Ourselin S, Royle G and McClelland JR 2015 Cone-Beam Computed Tomography and Deformable Registration-Based "Dose of the Day" Calculations for Adaptive Proton Therapy International Journal of Particle Therapy 2 404–14

Veiga C et al. 2016 First Clinical Investigation of Cone Beam Computed Tomography and Deformable Registration for Adaptive Proton Therapy for Lung Cancer International Journal of Radiation Oncology*Biology*Physics 95 549–59

van de Water S, Albertini F, Weber DC, Heijmen BJM, Hoogeman MS and Lomax AJ 2018 Anatomical robust optimization to account for nasal cavity filling variation during intensity-modulated proton therapy: a comparison with conventional and adaptive planning strategies Physics in Medicine & Biology 63 025020 [PubMed: 29160775]

van de Water S, van Dam I, Schaart DR, Al-Mamgani A, Heijmen BJM and Hoogeman MS 2016 The price of robustness; impact of worst-case optimization on organ-at-risk dose and complication probability in intensity-modulated proton therapy for oropharyngeal cancer patients Radiotherapy and Oncology 120 56–62 [PubMed: 27178142]

Wu Q, Chi Y, Chen PY, Krauss DJ, Yan D and Martinez A 2009 Adaptive Replanning Strategies Accounting for Shrinkage in Head and Neck IMRT International Journal of Radiation Oncology*Biology*Physics 75 924–32

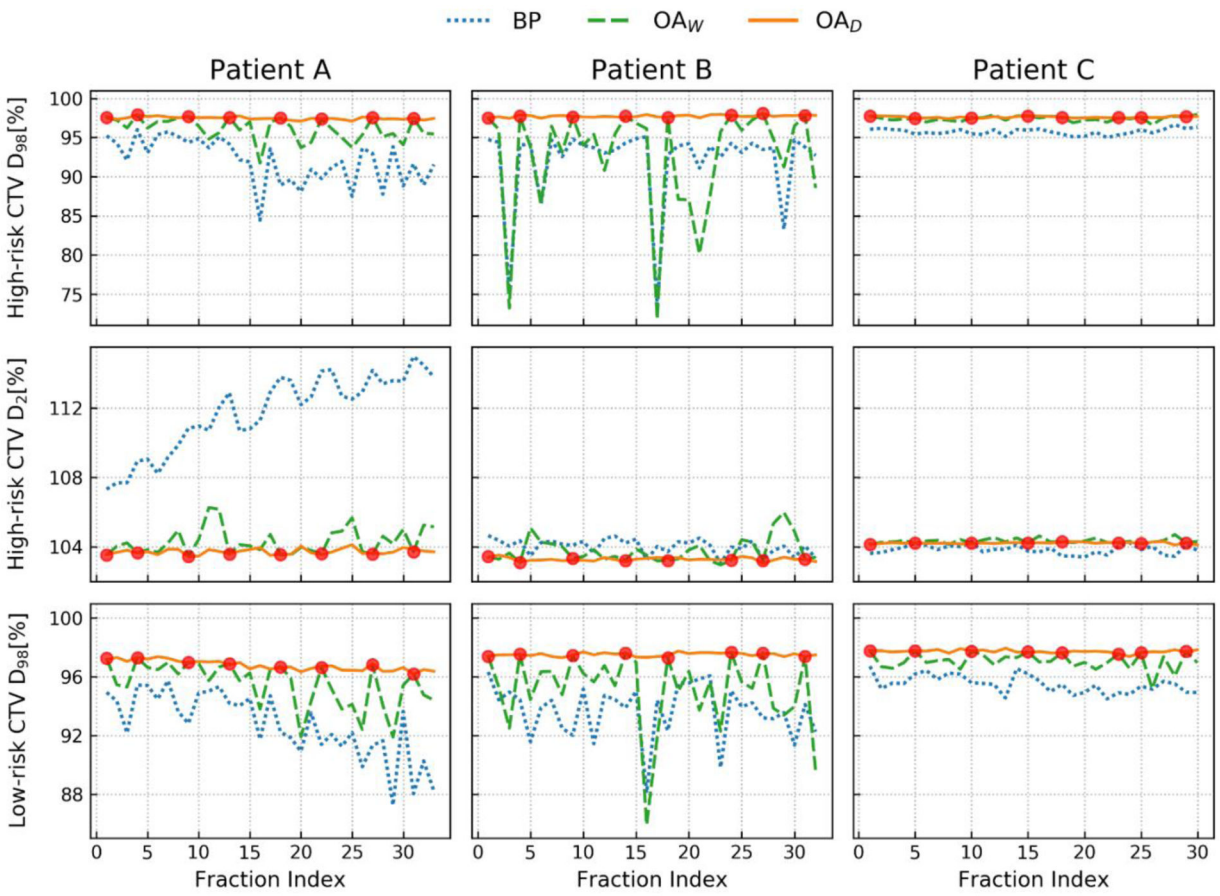


**Figure 1:**

Evolution of the target conformity (high-risk CTV and low-risk CTV) over the full course of treatment for a subset of three representative patients. The target coverage and overdose are evaluated using the $D_{98}$ and $D_2$, respectively (both in % of the prescription dose). The red dots represent which fractions of the $OA_W$ scenario were adapted. Overall, $OA_D$ achieves the best target coverage, while both $OA_D$ and $OA_W$ outperform BP.

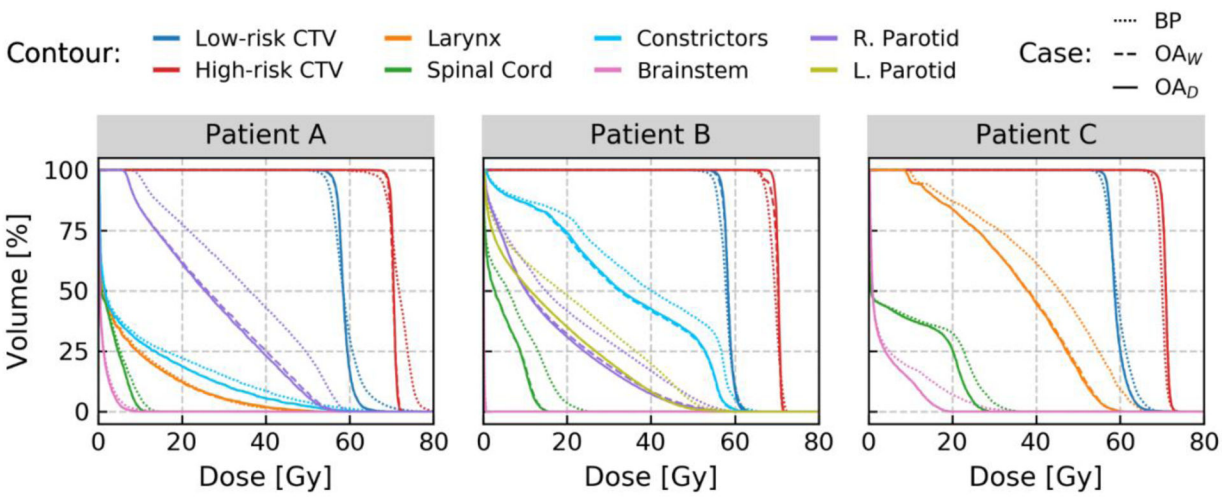


**Figure 2:**

DVHs for three representative patients, comparing the accumulated doses over the course of treatment, delivered by BP (dotted line), $OA_W$ (dashed line), and $OA_D$ (solid line). $OA_W$ yields remarkably similar performances to $OA_D$ for patients A and C, both in terms of target coverage and OAR sparing. For patient B, however, a clear difference regarding the high-risk CTV coverage can be observed between $OA_W$ and $OA_D$. In terms of target coverage, patient B exhibits the worst result for $OA_W$, which barely reached the clinical objective for the high-risk CTV. Both adaptation schemes improved the target coverage and decreased the dose to all OARs compared to BP.

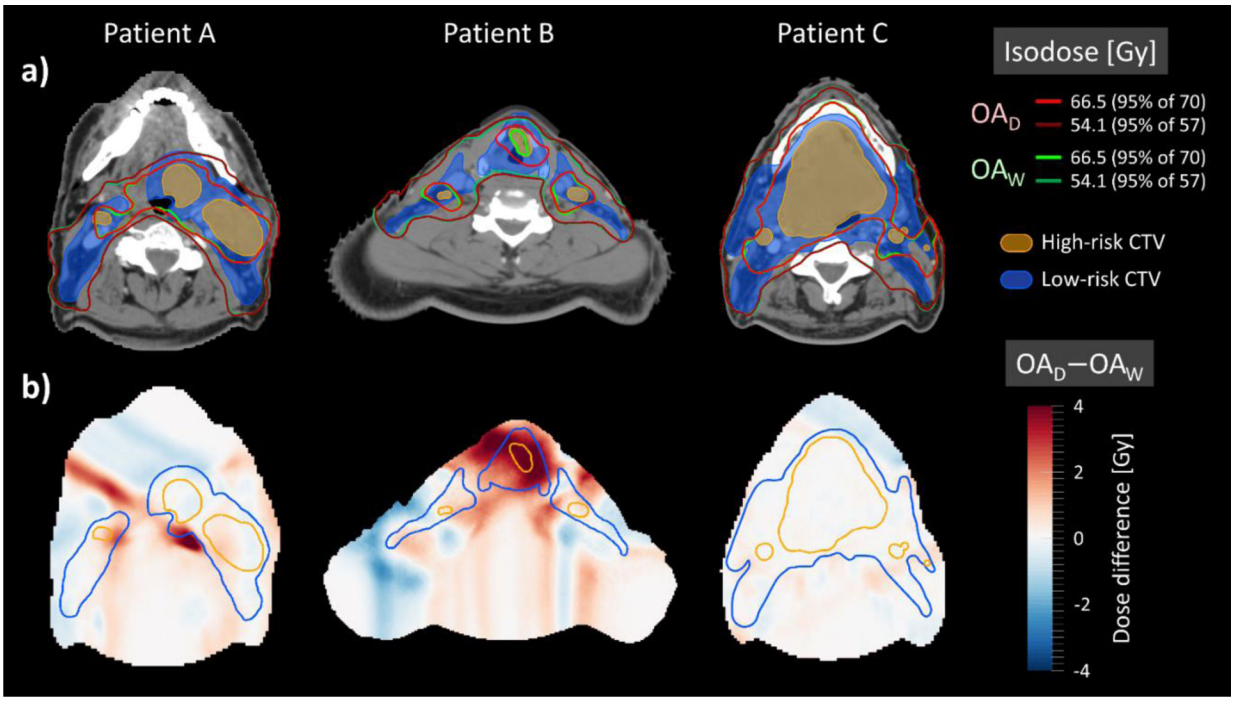


**Figure 3:**

**a)** Cumulative isodose lines of $OA_W$ and $OA_D$, each representing 95% of the prescription dose for the high-risk CTV and low-risk CTV (66.5 Gy and 54.1 Gy, respectively). The only noticeable difference between $OA_W$ and $OA_D$ can be observed for patient B, where $OA_W$ fails to cover part of the high-risk CTV. The remaining isodose lines mostly overlap, indicating similar accumulated dose distributions by $OA_W$ and $OA_D$. **b)** Dose difference maps ($OA_D$ minus $OA_W$) for the same CT slices. Differences of up to 4 Gy can be observed for patients A and B, whereby the latter case indicates underdosing in the high-risk CTV for $OA_W$. Patient C exhibits insignificant differences throughout the whole CT image set.

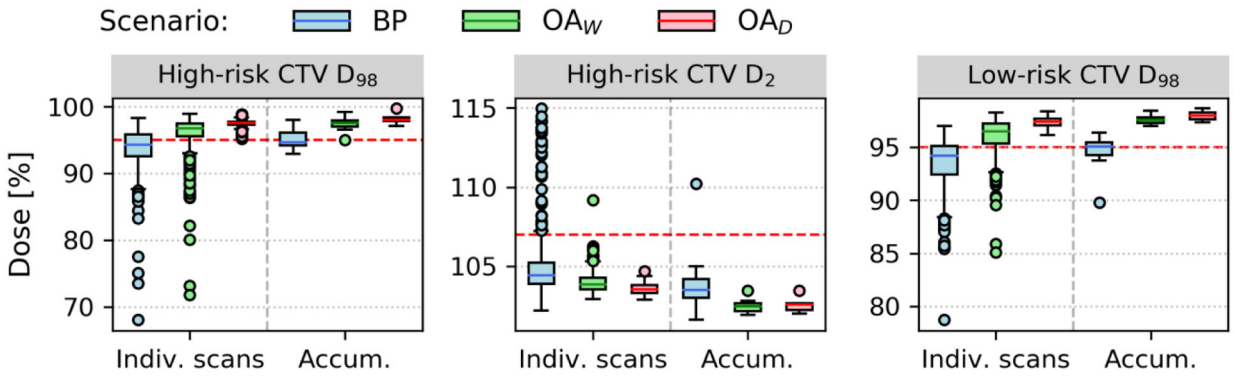


**Figure 4:**

Boxplots summarizing the metrics evaluated from the target (high-risk and low-risk CTV) DVHs for all ten patients, both for the dose delivered per individual fractions and for the dose accumulated throughout the treatment. The dashed red lines represent the defined clinical objectives regarding the target coverage. The boxplots include the median, the 1st and 3rd quartiles (25th and 75th percentiles) represented by the lower/upper hinges, the lower/upper whiskers extending from the corresponding hinges to the smallest/largest value no further than 1.5 times the inter-quartile range between the hinges, and individual outliers plotted beyond the whiskers.

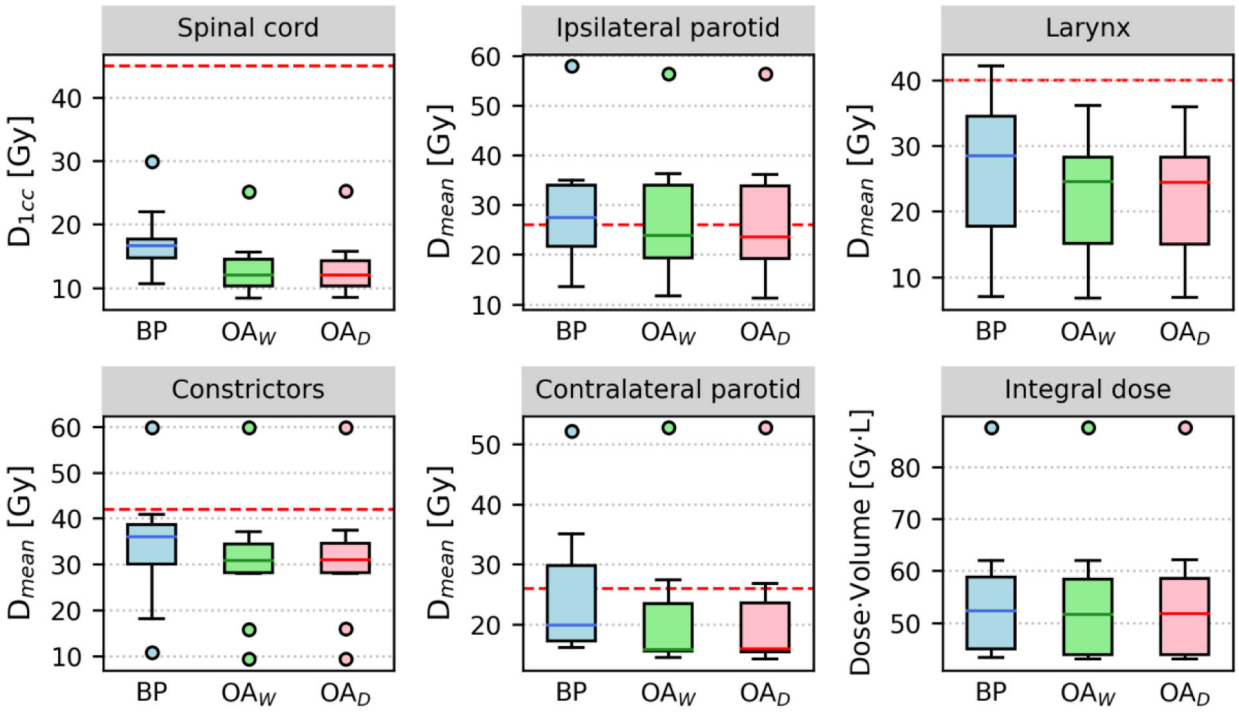


**Figure 5:**

Boxplots comparing the dose accumulated at the end of treatment for different OARs of all ten patients ($D_{mean}$ and $D_{1cc}$). The dashed red lines represent the clinical constraints defined for the corresponding OARs. Overall, both adaptation schemes perform similarly in terms of OAR sparing, while BP shows an increased dose for all structures.

**Table 1:**

Dose distribution statistics achieved in different structures (targets and OARs) for all ten patients by the three studied delivery scenarios.

| ROI | Metric | Objective | Dose | Scenario Median (min-max) | | |
|---|---|---|---|---|---|---|
| | | | | BP | $OA_W$ | $OA_D$ |
| High-risk CTV | $D_{98}$ [%] | ≥ 95% | Per frac.<br>Accum. | **94.28** (68.05–98.31)<br>**94.70** (92.96–98.06) | **96.73** (71.78–98.90)<br>**97.61** (95.02–99.26) | **97.56** (95.18–98.89)<br>**98.07** (97.15–99.73) |
| | $D_2$ [%] | ≤ 107% | Per frac.<br>Accum. | **104.40** (102.21–114.96)<br>**103.48** (101.60–110.22) | **103.84** (102.91–109.16)<br>**102.44** (101.91–103.47) | **103.54** (102.90–104.69)<br>**102.58** (102.00–103.45) |
| Low-risk CTV | $D_{98}$ [%] | ≥ 95% | Per frac.<br>Accum. | **94.21** (78.70–97.01)<br>**95.07** (89.76–96.39) | **96.52** (85.08–98.25)<br>**97.60** (97.03–98.43) | **97.40** (96.16–98.36)<br>**97.97** (97.34–98.65) |
| Spinal Cord | $D_{1cc}$ [Gy] | < 45 Gy | Accum. | **16.65** (10.60–29.89) | **11.99** (8.39–25.18) | **12.03** (8.50–25.26) |
| Brainstem | $D_{1cc}$ [Gy] | < 54 Gy | Accum. | **1.19** (0.47–24.71) | **0.97** (0.44–15.12) | **0.99** (0.43–15.08) |
| Ipsilateral Parotid | $D_{mean}$ [Gy] | < 26 Gy | Accum. | **27.44** (13.63–57.90) | **23.80** (11.69–56.31) | **23.60** (11.29–56.35) |
| Contralateral Parotid | $D_{mean}$ [Gy] | < 26 Gy | Accum. | **19.84** (16.20–52.12) | **15.74** (14.48–52.82) | **15.95** (14.21–52.81) |
| Larynx | $D_{mean}$ [Gy] | < 40 Gy | Accum. | **28.43** (7.01–42.13) | **24.48** (6.82–36.09) | **24.37** (6.92–35.89) |
| Constrictor Muscles | $D_{mean}$ [Gy] | < 42 Gy | Accum. | **36.05** (10.73–59.84) | **30.86** (9.26–59.81) | **30.90** (9.26–59.88) |
| Oral Cavity | $D_{mean}$ [Gy] | None | Accum. | **12.25** (6.83–52.65) | **12.35** (6.18–50.95) | **12.15** (6.21–51.20) |
| Healthy Tissue | Integral Dose [Gy*1] | None | Accum. | **52.34** (43.39–87.60) | **51.60** (43.04–87.54) | **51.76** (43.06–87.56) |